Research in Astron. Astrophys. **2012** Vol. **12** No. **4**, 383–399
http://www.raa-journal.org *http://www.iop.org/journals/raa*

***R**esearch in*
***A**stronomy and*
***A**strophysics*

Comparing the behavior of orbits in different 3D dynamical models for elliptical galaxies

Euaggelos E. Zotos

Department of Physics, Section of Astrophysics, Astronomy and Mechanics, Aristotle University of Thessaloniki 541 24, Thessaloniki, Greece; *evzotos@astro.auth.gr*

Received 2011 June 13; accepted 2012 January 9

Abstract We study the behavior of orbits in two different galactic dynamical models, describing the motion in the central parts of a triaxial elliptical galaxy with a dense nucleus. Numerical experiments show that both models display regular motion together with extended chaotic regions. A detailed investigation of the properties of motion is made for the 2D and 3D Hamiltonian systems, using a number of different dynamical parameters, such as the Poincaré surface of a section, the maximal Lyapunov Characteristic Exponent, the $S(c)$ spectrum, the $S(w)$ spectrum and the $P(f)$ indicator. The numerical calculations suggest that the properties of motion in both potentials are very similar. Our results show that one may use different kinds of gravitational potentials in order to describe the motion in triaxial galaxies while obtaining quantitatively similar results.

Key words: galaxies: kinematics and dynamics— galaxies: elliptical

1 INTRODUCTION

About forty years ago, the prevailing view was that elliptical galaxies were oblate spheroids flattened by rotation (see Sandage et al. 1970). It was the pioneering work of Bertola & Capaccioli (1975) and Illingworth (1977) that led astronomers to abandon the assumption that elliptical galaxies are necessarily oblate.

It is well known that observations of elliptical galaxies yield only the projected isophotes and, thus, determination of their intrinsic shapes requires statistical analysis, based on large samples (see Ryden 1996; Alam & Ryden 2002; Vincent & Ryden 2005) or mapping of potentials via detailed kinematical data for individual galaxies (see Davies et al. 2001; Rest et al. 2001; Statler et al. 2004).

Today it is believed that the shapes of elliptical galaxies are prolate or triaxial rather than oblate (see Benacchio & Galletta 1980; Binggeli 1980; Alam & Ryden 2002). On the other hand, kinematical studies of elliptical galaxies show evidence that triaxial galaxies do exist. Moreover, observational data indicate that most of the triaxial elliptical galaxies host a black hole or a dense nucleus in their centers (see Bak & Statler 2000; Statler et al. 2004). On this basis, we believe that it would be of interest to investigate the dynamical properties of a triaxial elliptical galaxy, particularly in its central region.

In order to describe the motion in the triaxial elliptical galaxy we use the well known logarithmic potential

$$V_{\rm g} = \frac{\upsilon_0^2}{2} \ln \left[x^2 + ay^2 + bz^2 + c_{\rm b}^2 \right] , \tag{1}$$

where υ_0 is used for the consistency of the galactic units, a and b are flattening parameters, and $c_{\rm b}$ is the scale length of the bulge component (see Binney & Tremaine 2008). Expanding potential (1) in a Taylor series about the origin and keeping terms up to the fourth degree in the variables, we find

$$V_{\rm g} = \frac{\upsilon_0^2}{2}\ln c_{\rm b}^2 + \frac{\upsilon_0^2}{2c_{\rm b}^2}\left(x^2+ay^2+bz^2\right) - \frac{\upsilon_0^2}{4c_{\rm b}^4}\left(x^2+ay^2+bz^2\right)^2 = \upsilon_0^2\ln c_{\rm b} + V_{\rm l}\,. \tag{2}$$

Thus the polynomial potential $V_{\rm l}$ is

$$V_{\rm l} = \frac{\upsilon_0^2}{2c_{\rm b}^2}\left(x^2+ay^2+bz^2\right) - \frac{\upsilon_0^2}{4c_{\rm b}^4}\left(x^2+ay^2+bz^2\right)^2\,, \tag{3}$$

where it was assumed that

$$\frac{x^2+ay^2+bz^2}{c_{\rm b}^2} \ll 1\,. \tag{4}$$

The reader can find more details about the Taylor expansion of the logarithmic potential in Zotos (2011b). To potentials (1) and (3) we add the potential of a spherically symmetric nucleus

$$V_{\rm n} = \frac{-M_{\rm n}}{\sqrt{x^2+y^2+z^2+c_{\rm n}^2}}\,, \tag{5}$$

where $M_{\rm n}$ is the nuclear mass, while $c_{\rm n}$ is the scale length of the nucleus. We apply a Plummer sphere, in order to increase the central mass of the galaxy. This method has been applied several times in previous works, having as an objective to study the effects of the introduction of a central mass component in a galaxy (see Hasan & Norman 1990; Hasan et al. 1993).

The aim of the present article is to investigate the properties of motion near the center of a triaxial elliptical galaxy described by potentials (1) and (3) with an additional dense nucleus described by potential (5). In particular, we are interested to study the regular or chaotic character of motion in both of the above described potentials, in order to be able to compare the corresponding results. Furthermore, we shall compare the density in the central parts of the triaxial galaxy derived using the two potentials described above. In order to achieve a better picture for the properties of motion, we first investigate the 2D system, that is when $z = 0$, and then we will use the corresponding results to study the dynamical system of three (3D) degrees of freedom.

From the pioneering work of Henon & Heiles (1964) there has been an ongoing interest in finding new methods, in order to distinguish between ordered and chaotic motion in dynamical systems. The Poincaré surface of section (PSS) for the two dimensional (2D) systems and the Lyapunov Characteristic Exponent (LCE) (Benettin et al. 1976; Froeschle 1984; Lichtenberg & Lieberman 1992) for dynamical systems with any degree of freedom are two well known methods to characterize an orbit as regular or chaotic. Over the last thirty years, an effort has been made in order to find new, modern and also reliable and fast ways to detect the chaotic behavior in galactic systems. One could mention the frequency map analysis developed by Laskar (Laskar et al. 1992; Laskar 1993), the dynamical spectra of stretching numbers (the distribution of values of a given parameter along the obit), introduced by Froeschle (1984) (see also Froeschle et al. 1993; Voglis & Contopoulos 1994; Contopoulos et al. 1995; Contopoulos et al. 1997) and the $P(f)$ spectral method applied and used by Karanis & Vozikis (2008). In the present research, we use, apart from the classical PSS technique and the LCE, some modern methods such as the $S(c)$ and $S(w)$ dynamical spectra and the $P(f)$ indicator.

Here, we must provide some additional theoretical information regarding these new dynamical methods. We use the $S(c)$ spectrum in order to characterize the nature of an orbit in a 2D dynamical system. This spectrum has been proved to be a very reliable tool in several cases (see Caranicolas & Papadopoulos 2007; Zotos 2011a). The nature of a 2D orbit can be revealed by looking at the

shape of the $S(c)$ spectrum. If the shape of the spectrum is a well defined U-type structure, then the corresponding orbit is regular. On the other hand, if the shape is complicated and highly asymmetric, with a lot of large and small abrupt peaks, then the orbit is chaotic. Moreover, the $S(c)$ spectrum can help us identify resonant orbits of higher multiplicity, as it produces as many U-type structures as the total number of islands of the invariant curves on the $x - p_x$ phase plane. One more advantage of this spectrum is that it can be deployed in order to calculate the sticky period of a 2D orbit and also to follow its time evolution towards the chaotic sea (see fig. 5 in Zotos 2011a).

For the study of 3D orbits, we use the $S(w)$ spectrum. By definition this spectrum is based on a complicated combination of the coordinates and the momenta of the 3D orbit. In particular, this spectrum is an advanced form of the $S(c)$ spectrum and therefore carries all the characteristics mentioned in the previous paragraph regarding the pattern of the spectrum for regular and chaotic orbits. The only difference is that in this case the $S(w)$ spectrum produces as many U-type structures as the total number of invariant 3D tori in the (x, p_x, z) phase space. We introduced this new spectrum definition in Zotos (2011a), in order to construct a new spectral definition appropriate for the study of 3D orbits.

The Fourier Transform is usually defined as a transformation of a quantity q which is a function of time, $q(t)$, with regard to its respective function of amplitude p, which is a function of frequency $P(f)$. We can define a series of time intervals between successive crossings over a section. Then we calculate the Power Spectrum of these time intervals, using a Discrete Fast Fourier Transformation (FFT) algorithm. Looking at the $P(f)$ spectrum of a regular 2D or 3D orbit, we expect to observe a smooth curve, with some additional peaks corresponding to the "periodicities" of the time series. On the contrary, in a 2D or 3D chaotic orbit no such "periodicities" exist and therefore its $P(f)$ spectrum will produce a very "noisy" pattern with a large number of peaks which would be very densely distributed. One of the main advantages of this spectral method is that is uses only one orbit and we do not need to trace the behavior of any nearby orbit. Furthermore, the detection can be made quite early using less iterations, compared to the iterations needed to reach a conclusive result using the LCE. More detailed information regarding this method and its applications can be found in Karanis & Vozikis (2008).

Here we must remind the reader that the $S(c)$ spectrum is the distribution function of the parameter c

$$S(c) = \frac{\Delta N(c)}{N \Delta c}\,, \tag{6}$$

where $\Delta N(c)$ are the numbers of the parameters c in the interval $(c, c + \Delta c)$ after N iterations. The parameter c is defined as

$$c_i = \frac{x_i - p_{xi}}{p_{yi}}\,, \tag{7}$$

where (x_i, p_{xi}, p_{yi}) are the successive values of the (x, p_x, p_y) elements of the 2D orbits, on the Poincaré $x - p_x, y = 0, p_y > 0$ phase plane. More details regarding the $S(c)$ spectrum and its applications can be found in Caranicolas & Papadopoulos (2007) and Caranicolas & Zotos (2010).

The Hamiltonian corresponding to the potential (1) or (3) is written as

$$H = \frac{1}{2}\left(p_x^2 + p_y^2 + p_z^2\right) + V_{\rm t}\left(x, y, z\right) = E\,, \tag{8}$$

where $V_{\rm t}$ represents $V_{\rm tg} = V_{\rm g} + V_{\rm n}$ or $V_{\rm tl} = V_{\rm l} + V_{\rm n}$. Here p_x, p_y and p_z are the momenta per unit mass conjugate to x, y and z respectively, while E is the numerical value of the Hamiltonian (8), which is conserved.

In this article, we use a system of galactic units, where the unit of length is 1kpc, the unit of mass is $2.325 \times 10^7 M_\odot$ and the unit of time is 0.97748×10^8 yr. The velocity unit is 10 km s^{-1}, while G is equal to unity. In the above units we use the values: $\upsilon_0 = 10, c_{\rm b} = 3, M_{\rm n} = 10, c_{\rm n} = 0.1, a = 1.5$ and $b = 1.7$.

The results of the present research are based on the numerical integration of the equations of motion

$$\begin{aligned} \ddot{x} &= -\frac{\partial V_{\rm t}(x,y,z)}{\partial x}\,, \\ \ddot{y} &= -\frac{\partial V_{\rm t}(x,y,z)}{\partial y}\,, \\ \ddot{z} &= -\frac{\partial V_{\rm t}(x,y,z)}{\partial z}\,, \end{aligned} \tag{9}$$

which was made using a Bulirsh-Stöer routine in Fortran 95, with double precision in all subroutines. The accuracy of the calculations was checked by the constancy of the energy integral (8), which was conserved up to the eighteenth significant figure.

This paper is organized as follows. In Section 2 we present and compare the results for the 2D systems. In Section 3 we compare the mass density near the center derived using the two 3D potentials. Moreover, we compare the properties of the 3D orbits in the two dynamical models. In Section 4, the conclusions and the discussion of our results are presented.

2 RESULTS FOR THE 2D DYNAMICAL SYSTEMS

In this section, we study the character of orbits in the 2D dynamical systems. In this case, we set $z = p_z = 0$ in (8) and the corresponding 2D Hamiltonian is

$$H_2 = \frac{1}{2}\left(p_x^2 + p_y^2\right) + V_{\rm t}\left(x,y\right) = E_2\,, \tag{10}$$

where E_2 is the numerical value of the Hamiltonian. As the phase space of the system is four dimensional we use the $x - p_x, y = 0, p_y > 0$ Poincaré phase plane. The results are presented in Figures 1 and 2.

Figure 1 shows the phase plane for potential $V_{\rm tg}$, while Figure 2 shows the phase plane for potential $V_{\rm tl}$. Here, we must emphasize that the two phase planes were constructed for values of energies connected by the relation

$$E_{\rm 2tg} = E_{\rm 2tl} + \upsilon_0^2 \ln c_{\rm b} \tag{11}$$

and the same initial conditions, in order to be able to make the comparison. Here we took $E_{\rm 2tl} = -4.70, \upsilon_0^2 \ln c_{\rm b} = 109.86$, which gives the value 105.16 for $E_{\rm 2tg}$. As one can see, the two phase planes are almost identical. In both figures, we see areas of regular motion and extended chaotic regions. There are three main families of regular orbits. (i) Orbits producing invariant curves around each of the two stable 1:1 resonant periodic points. (ii) Orbits producing a set of three islands - one of them is on the x-axis, while the other two are symmetric with respect to the p_x axis. These orbits are characteristic of the 3:3 resonance. (iii) Box orbits producing invariant curves surrounding the whole chaotic sea. Note that the area on the $x - p_x$ phase planes occupied by each of the above families of regular orbits is quantitatively the same in both Figures 1 and 2. In addition to the regular orbits there are also a large number of irregular orbits producing a large, unified chaotic sea. Note that the extent of the chaotic sea is almost the same in both phase planes. The differences between the two phase planes produced by potentials $V_{\rm tg}$ and $V_{\rm tl}$ are negligible and they are confined to some tiny islands, embedded inside the chaotic sea. These tiny islands are produced by secondary resonances.

In order to investigate and compare in detail the properties of motion in both potentials, we present and compare in the following a number of orbits belonging to different families of orbits.

Figure 3(a)–(d) shows results for a regular orbit in potential $V_{\rm tg}$. The orbit shown in Figure 3(a) belongs to family (i) and has initial conditions: $x_0 = 0.5, y_0 = 0, p_{x0} = 0$, while in all cases,

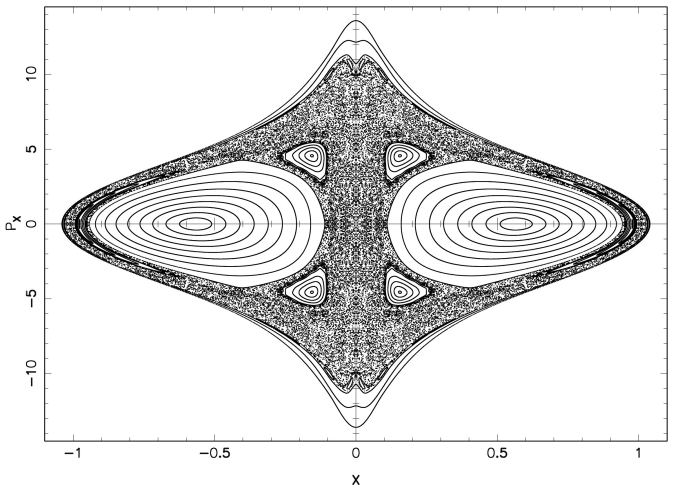

Fig. 1 The $x - p_x$ phase plane for the potential $V_{\rm tg}$, when $\upsilon_0 = 10, c_{\rm b} = 3, M_{\rm n} = 10, c_{\rm n} = 0.1, a = 1.5, b = 1.7$ and $E_{\rm 2tg} = 105.16$.

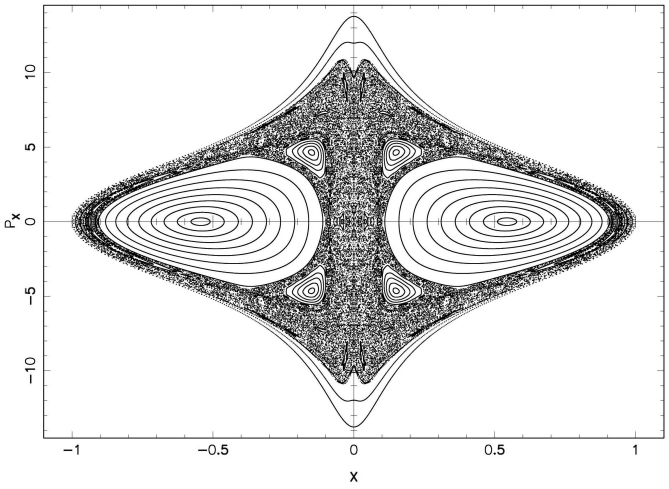

Fig. 2 Similar to Fig. 1, but for the potential $V_{\rm tl}$. The value of energy is $E_{\rm 2tl} = -4.70$.

p_{y0} is found from the energy integral (10). The corresponding values of energy and all the other parameters are as in Figure 1. Figure 3(b) shows the maximum LCE of the orbit, which vanishes indicating regular motion. Figure 3(c) shows the $S(c)$ spectrum of the orbit. Here, we see a well defined U type spectrum characteristic of the regular motion. In Figure 3(d), we see a plot of the $P(f)$ indicator, which displays only two peaks indicating regular motion. In order to help the reader, we note that the orbit shown in Figure 3(a) was calculated for a time period of 100 time units. The time scale for the $S(c)$ spectrum and the $P(f)$ indicator was $10^3 - 10^4$ time units.

Figure 4(a)–(d) shows results for an orbit, with the same initial conditions and with the same time scales for all calculations, but for the potential $V_{\rm tl}$. All other parameters are the same as in Figure 2.

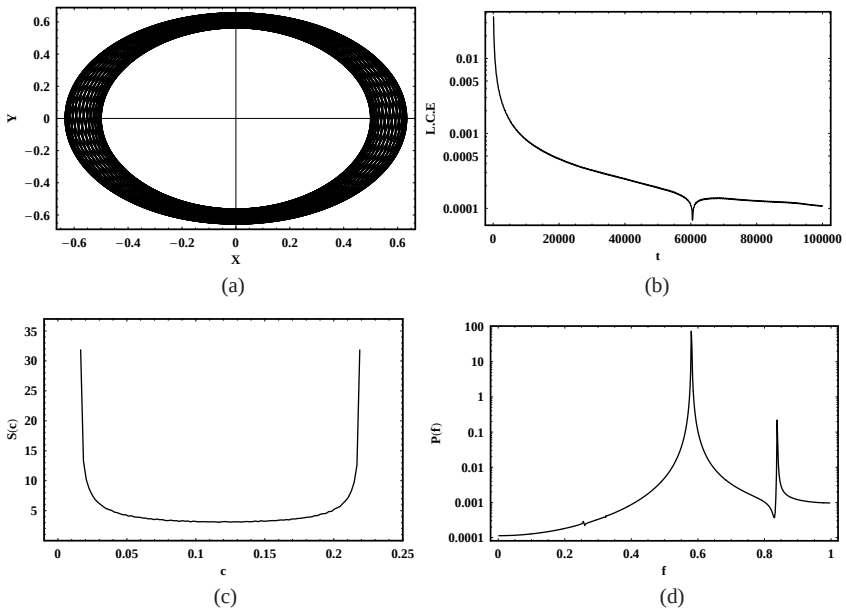

(a) (b) (c) (d)

Fig. 3 (a) A regular orbit in the 2D potential $V_{\rm tg}$. Initial conditions are: $x_0 = 0.5, y_0 = 0, p_{x0} = 0$, while p_{y0} is found from the energy integral. The values of all other parameters and energy are as in Fig. 1. (b) A plot of the maximum LCE vs. time for the orbit shown in (a). (c) The $S(c)$ spectrum of the orbit shown in (a) and (d) The $P(f)$ indicator for the orbit shown in (a).

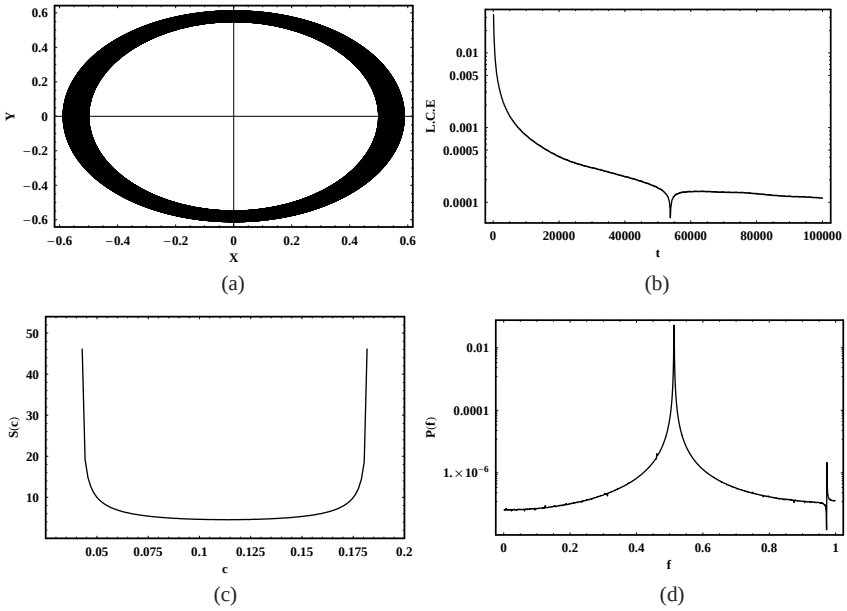

(a) (b) (c) (d)

Fig. 4 (a)–(d): Similar to Fig. 3(a)–(d) for the potential $V_{\rm tl}$. The values of all other parameters and energy are the same as in Fig. 2.

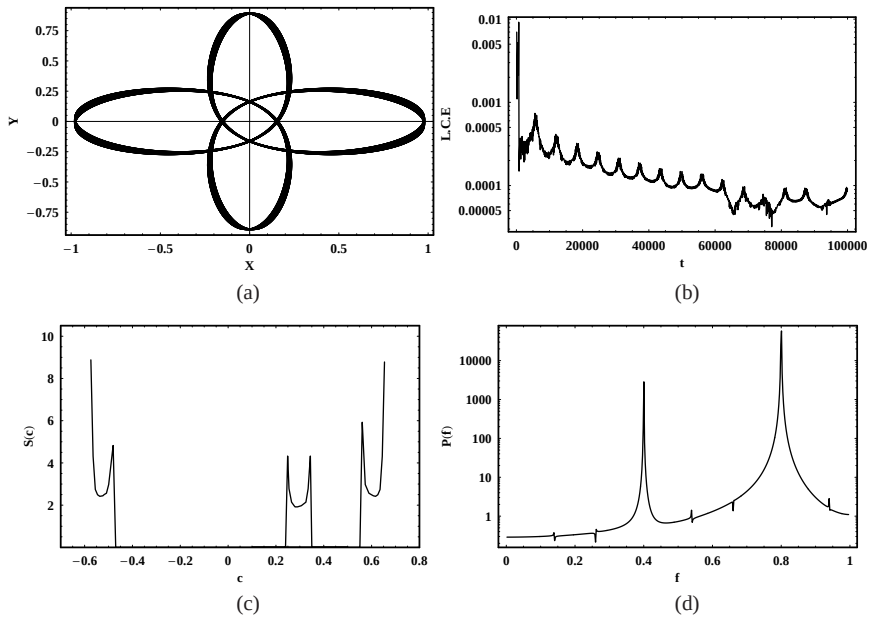

Fig. 5 (a)–(d): Similar to Fig. 3(a)–(d) for a resonant orbit. Initial conditions are: $x_0 = 0.15, y_0 = 0, p_{x0} = 4.5$. The values of all other parameters and energy are the same as in Fig. 1.

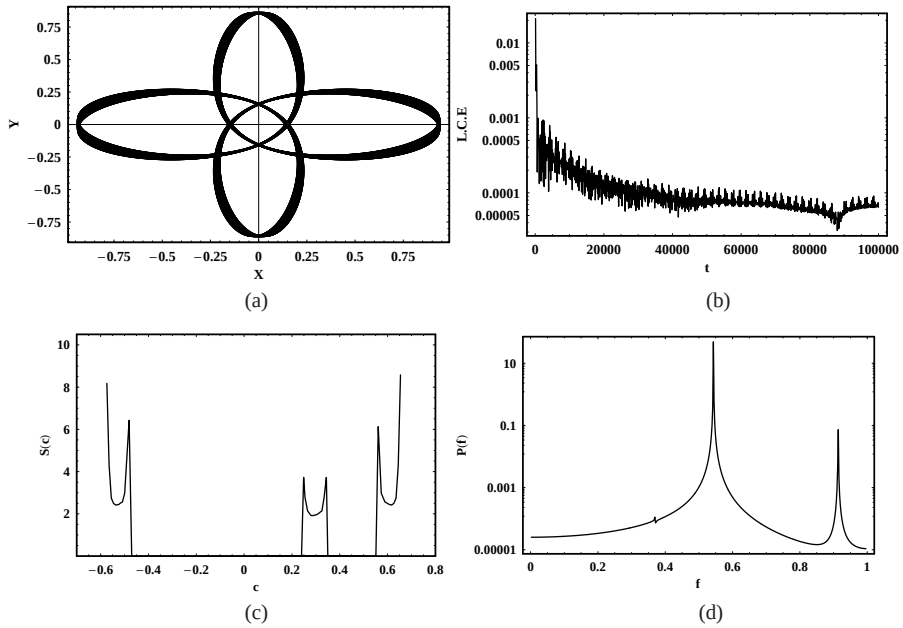

Fig. 6 (a)–(d): Similar to Fig. 5(a)–(d) for the potential $V_{\rm t1}$. The values of all other parameters and energy are the same as in Fig. 2.

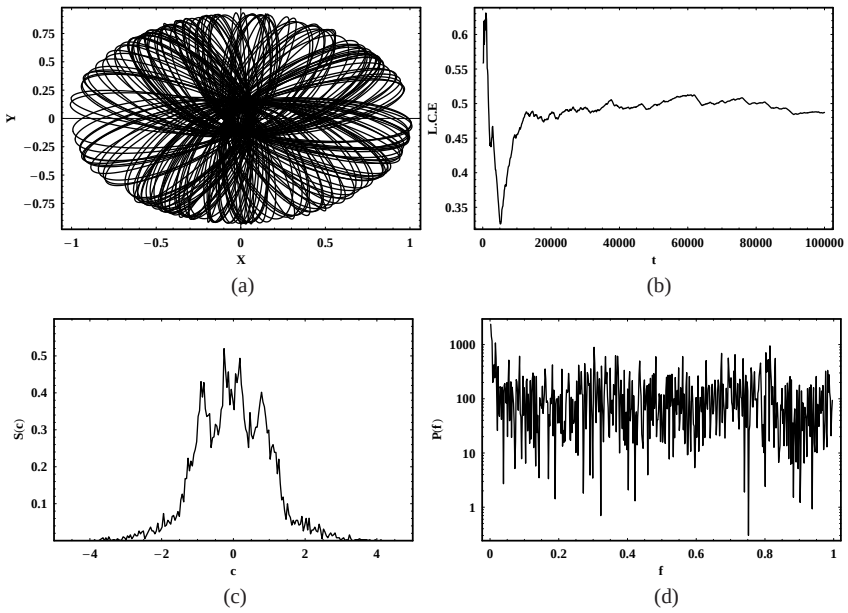

Fig. 7 (a)–(d): Similar to Fig. 3(a)–(d) for a chaotic orbit. Initial conditions are: $x_0 = 0.02, y_0 = 0, p_{x0} = 2.5$. The values of all other parameters and energy are the same as in Fig. 1.

In order to have a better picture of the properties of motion in the two potentials $V_{\rm tg}$ and $V_{\rm tl}$, we present results for two more orbits.

Figures 5(a)–(d) and 6(a)–(d) are similar to 3(a)–(d) and 4(a)–(d), for an orbit with initial conditions: $x_0 = 0.15, y_0 = 0, p_{x0} = 4.5$. This orbit belongs to family (ii) and it is characteristic of the 3:3 resonance. As one can see, the outcomes presented in the two figures are very similar. The results presented in Figures 7(a)–(d) and 8(a)–(d) are similar to those of Figures 3(a)–(d) and 4(a)–(d) but for a chaotic orbit. Initial conditions are: $x_0 = 0.02, y_0 = 0, p_{x0} = 2.5$. Here the maximum LCE has a positive value indicating chaotic motion. Moreover, the $S(c)$ spectrum shows a number of large and small peaks which is characteristic of chaotic motion. Finally, the $P(f)$ indicator is highly asymmetric with a large number of peaks, also indicating chaotic motion. Comparing the results given in Figures 7(a)–(d) and 8(a)–(d), we can say that they are very similar.

Given all the above, we can say that our numerical results, which are obtained by several different dynamical methods using regular and chaotic orbits, strongly suggest that the potential $V_{\rm tl}$ satisfactorily describes the properties of motion of the potential $V_{\rm tg}$ near the center of a triaxial, elliptical galaxy. Since the potential of the spherical nucleus $V_{\rm n}$ is the same in both potentials $V_{\rm tg}$ and $V_{\rm tl}$, this means that no information is lost when we go from a global triaxial logarithmic potential (1) to the local polynomial potential (2). Remember that this only holds near the center of the galaxy, when (4) is valid. In order to investigate and compare the character of motion in the two 2D potentials $V_{\rm tg}$ and $V_{\rm tl}$, we have computed a large number of orbits - about 1000 - with different initial conditions (x_0, p_{x0}), but with the same initial conditions in both 2D potentials. In particular, as we have in both cases regular regions and only one unified chaotic sea in each $x - p_x$ phase plane, we calculate the maximum value of the LCE by choosing 500 orbits with different and random initial conditions (x_0, p_{x0}) in the regular regions and 500 orbits with different and random initial conditions (x_0, p_{x0}) in the chaotic sea in each case. Our numerical experiments show that the vast majority of orbits - about 97.4% - displayed the same characteristics, including the same nature of

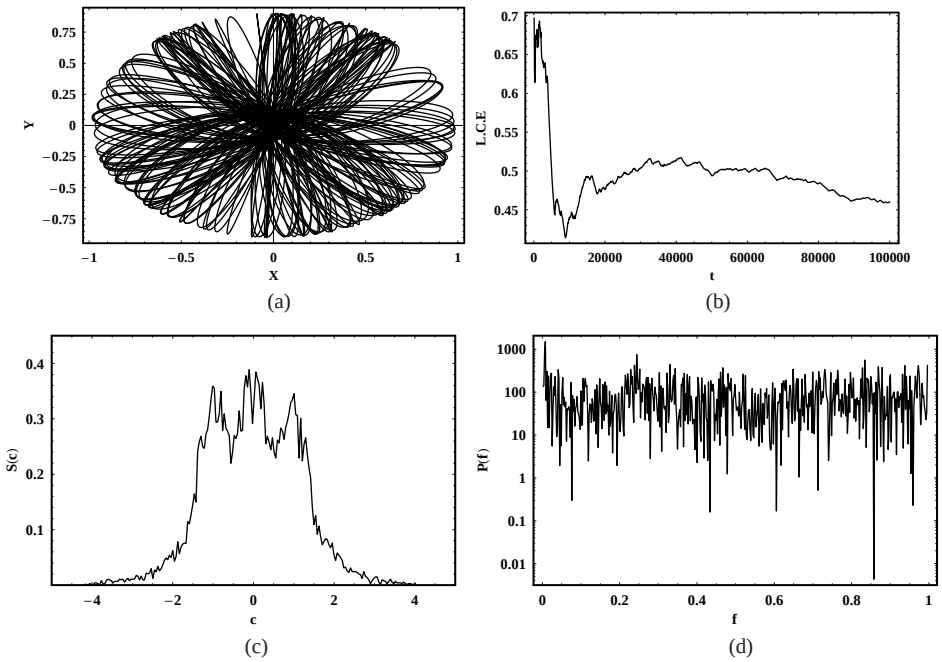

Fig. 8 (a)–(d): Similar to Fig. 7(a)–(d) for the potential $V_{\rm tl}$. The values of all other parameters and energy are the same as in Fig. 2.

orbit, maximum LCE, $S(c)$ spectrum and $P(f)$ indicator, while only 2.6% of the tested orbits were different.

3 RESULTS FOR THE 3D DYNAMICAL SYSTEMS

We now proceed to study the properties of motion in the 3D potentials. Before doing this, it would be interesting to compare the mass densities derived from the 3D potentials $V_{\rm tg}$ and $V_{\rm tl}$. The mass density can be found using Poisson's law

$$\nabla^2 V_{\rm t} = 4\pi G \rho_t \,, \tag{12}$$

where $V_{\rm t}$ represents $V_{\rm tg} = V_{\rm g} + V_{\rm n}$ or $V_{\rm tl} = V_{\rm l} + V_{\rm n}$, while ρ_t represents ρ_{tg} or ρ_{tl}.

Figure 9(a)–(h) shows the surfaces of equal density for the 3D potentials $V_{\rm tg}$ and $V_{\rm tl}$. We can see that the results are very similar. In order to compare the mass density from another point of view, we present in Figure 10 (a)–(f) the contours of equal density in the xy, xz and yz planes respectively for the two potentials. As is understood, these contours are the projections of the four surfaces of equal density to the three principal planes xy, xz and yz. Here we can visualize that the deviations between the mass density of the two potentials are extremely small and therefore negligible.

Let us now come to investigate and compare the orbits in the two 3D potentials. For this purpose, we apply the $S(w)$ dynamical spectrum, which was introduced in Zotos (2011a), in order to distinguish between ordered and chaotic motion in 3D dynamical systems. The parameter w_i is defined as

$$w_i = \frac{(x_i - p_{xi}) - (z_i - p_{zi})}{p_{yi}} \,, \tag{13}$$

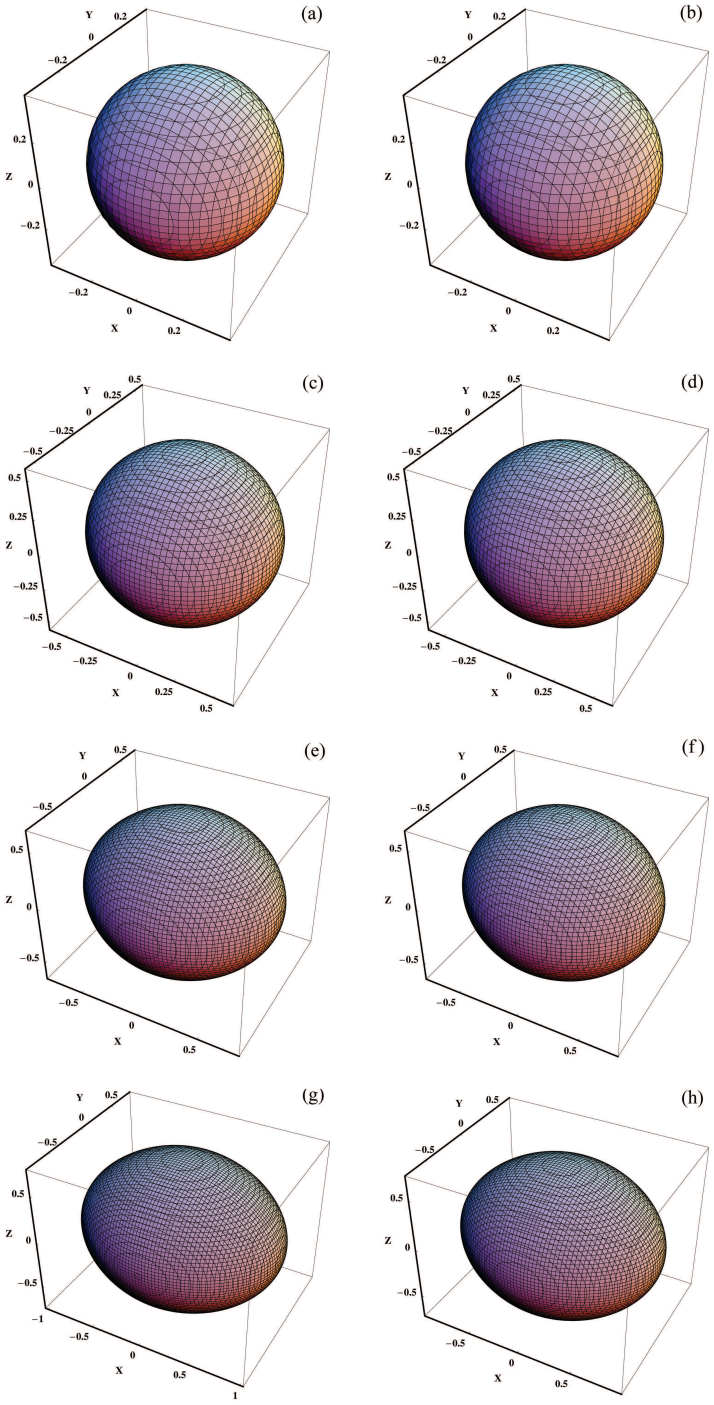

Fig. 9 (a)–(h): Surfaces of equal density for the 3D potentials. Left patterns correspond to potential $V_{\rm tg}$, while right patterns to potential $V_{\rm tl}$.

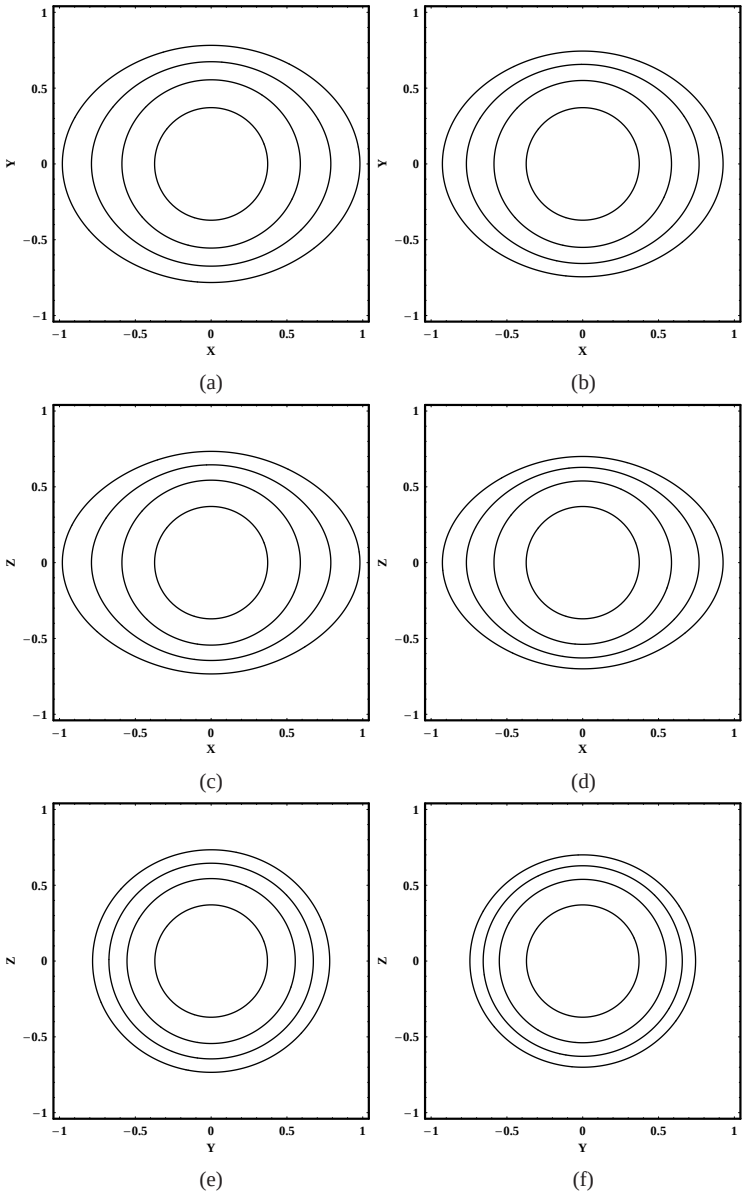

Fig. 10 (a)–(f): Contours of equal density in the xy, xz and yz planes. Left patterns correspond to potential $V_{\rm tg}$, while right patterns to potential $V_{\rm tl}$.

where $(x_i, z_i, p_{xi}, p_{yi}, p_{zi})$ are the successive values of the (x, z, p_x, p_y, p_z) elements of the 3D orbits. The dynamical spectrum of the parameter w is its distribution function

$$S(w) = \frac{\Delta N(w)}{N \Delta w}\,, \tag{14}$$

where $\Delta N(w)$ is the number of parameters w in the interval $(w, w + \Delta w)$ after N iterations. In order to study the character of a 3D orbit, the $S(c)$ spectrum can also be applied. Note that the

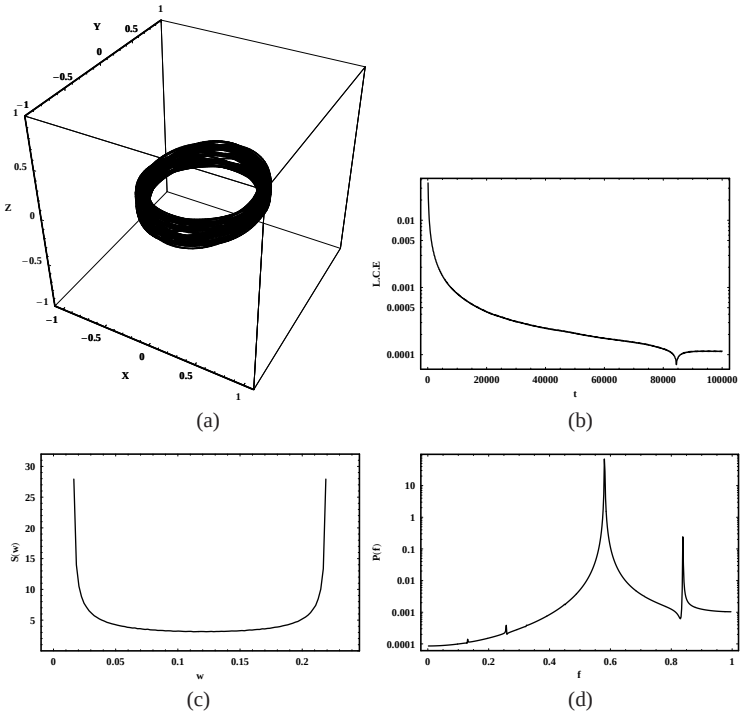

Fig. 11 (a) A regular orbit in the 3D potential $V_{\rm tg}$. Initial conditions are: $x_0 = 0.5, y_0 = 0, p_{x0} = 0, z_0 = 0.1$, while p_{y0} is found from the energy integral. The values of all other parameters and energy are as in Fig. 1. (b) A plot of the maximum LCE vs time for the orbit shown in (a). (c) The $S(w)$ spectrum of the orbit shown in (a). (d) The $P(f)$ indicator for the orbit shown in (a).

coupling of the third component z, carrying all the information regarding the 3D motion, is hidden in the definition of the $S(c)$ spectrum, but in any case it affects the values of x, p_x and p_y. Using the definition of the $S(w)$ spectrum, we overcome this minor drawback as we deploy an improved dynamical spectrum, especially suitable for 3D orbits.

Figure 11(a)–(d) shows the results for a 3D regular orbit in potential $V_{\rm tg}$. The orbit which is shown in Figure 11(a), has initial conditions: $x_0 = 0.5, y_0 = p_{x0} = p_{z0} = 0, z_0 = 0.1$, while for all 3D orbits the value of p_{y0} is found from the energy integral (8). The corresponding values of all the other parameters are the same as in Figure 1. The value of energy is $E_{tg} = 105.16$, the same as in the 2D system. The maximum LCE of this orbit, which is shown in Figure 11(b), vanishes indicating regular motion. Figure 11(c) shows the $S(w)$ spectrum of the orbit. This is a well defined U type spectrum characteristic of the regular motion. In Figure 11(d) we can see the $P(f)$ indicator which also indicates regular motion. Figure 12(a)–(d) shows results for the same orbit but in the potential $V_{\rm tl}$. The values of the other parameters are the same as in Figure 2. The value of energy is $E_{tl} = -4.70$, the same as in the 2D system. Comparing the two Figures 11(a)–(d) and 12(a)–(d) we see that the results are very similar.

Figures 13(a)–(d) and 14(a)–(d) are similar to Figures 11(a)–(d) and 12(a)–(d) for a resonant 3D orbit with initial conditions: $x_0 = 0.15, y_0 = 0, p_{x0} = 4.5, p_{z0} = 0, z_0 = 0.01$. The similarity between the two patterns is evident. Finally, in Figures 15(a)–(d) and 16(a)–(d), we present results for a chaotic 3D orbit. The initial conditions are: $x_0 = 0.02, y_0 = 0, p_{x0} = 2.5, p_{z0} = 0, z_0 = 0.1$. The values of energy and other parameters are as in Figure 13(a)–(d) and 14(a)–(d) respectively. Again we see that the results are very similar.

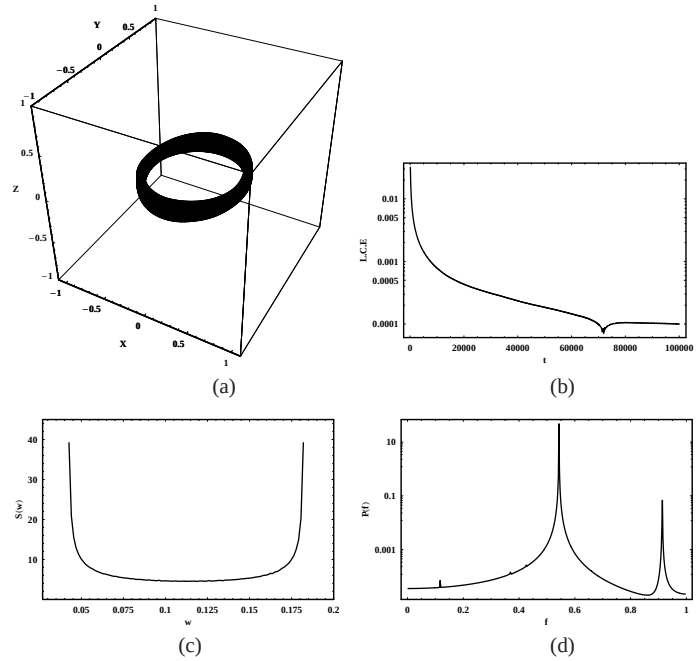

(a) (b) (c) (d)

Fig. 12 (a)–(d): Similar to Fig. 11(a)–(d) for the potential $V_{\rm tl}$. The values of all other parameters and energy are the same as in Fig. 2.

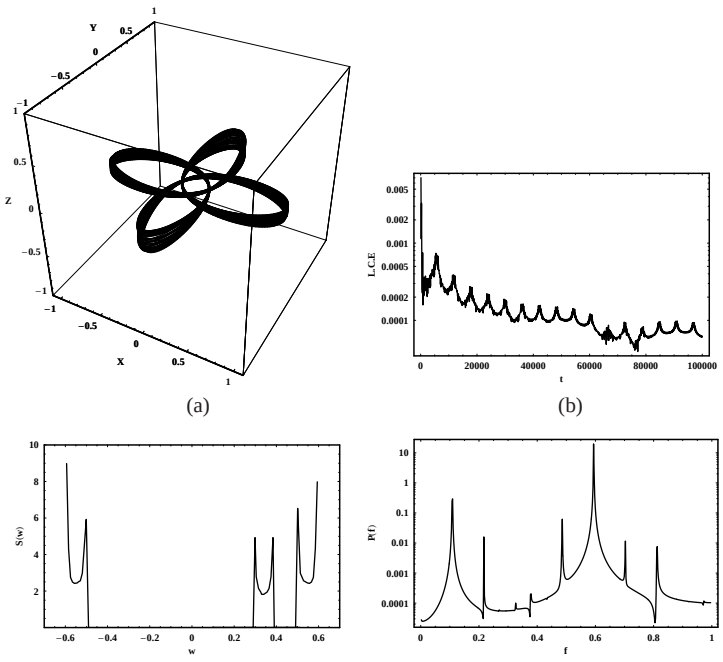

(a) (b) (c) (d)

Fig. 13 (a)–(d): Similar to Fig. 11(a)–(d) for a resonant 3D orbit. Initial conditions are: $x_0 = 0.15, y_0 = 0, p_{x0} = 4.5, z_0 = 0.01$. The values of all other parameters and energy are the same as in Fig. 1.

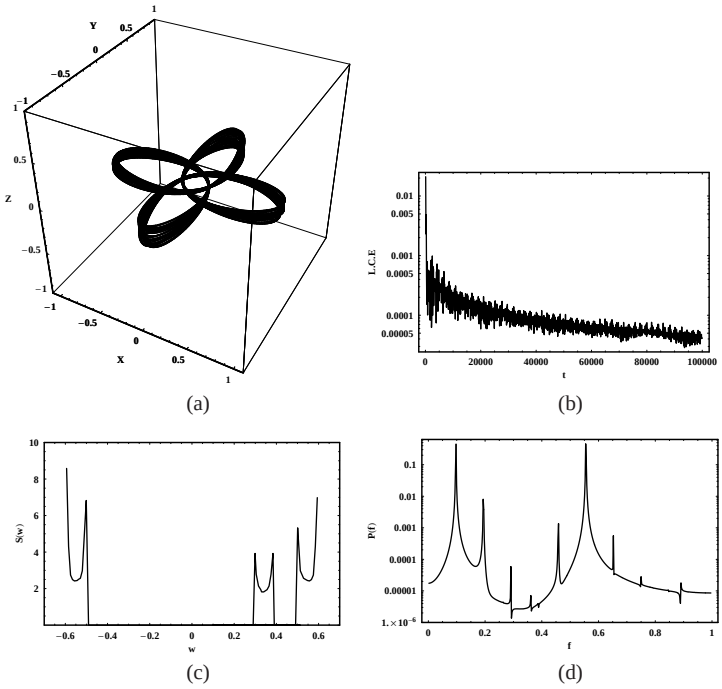

(a) (b) (c) (d)

Fig. 14 (a)–(d): Similar to Fig. 13(a)–(d) for the potential $V_{\rm tl}$. The values of all other parameters and energy are the same as in Fig. 2.

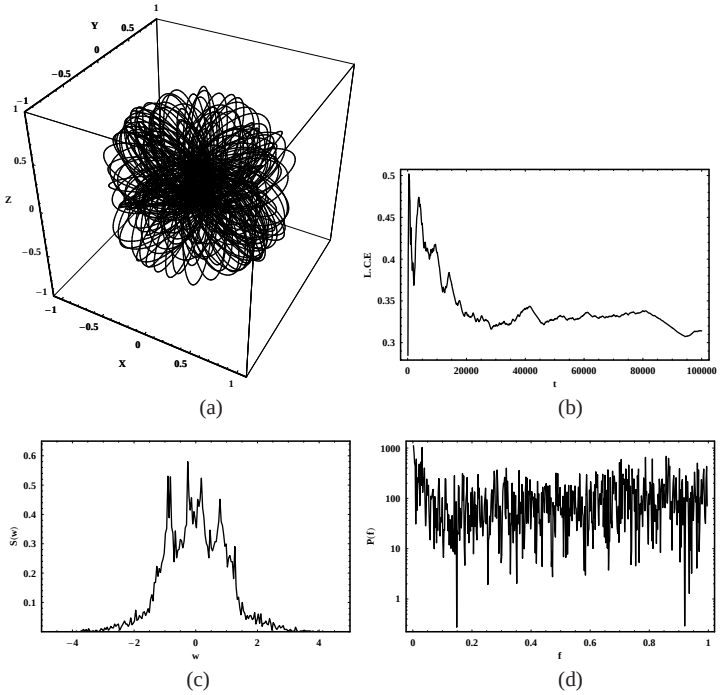

(a) (b) (c) (d)

Fig. 15 (a)–(d): Similar to Fig. 11(a)–(d) for a chaotic 3D orbit. Initial conditions are: $x_0 = 0.02, y_0 = 0, p_{x0} = 2.5, z_0 = 0.1$. The values of all other parameters and energy are the same as in Fig. 1.

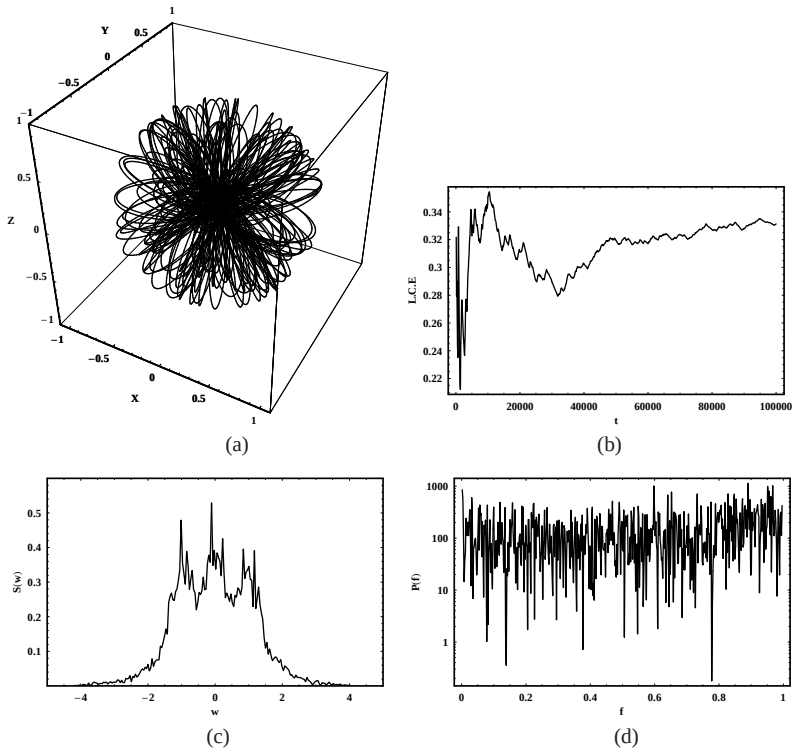

Fig. 16 (a)–(d): Similar to Fig. 15(a)–(d) for the potential $V_{\rm tl}$. The values of all other parameters and energy are the same as in Fig. 2.

In order to investigate and compare the characteristics of motion in the two 3D potentials $V_{\rm tg}$ and $V_{\rm tl}$, we work as follows. We use initial conditions $(x_0, p_{x0}, z_0), y_0 = p_{z0} = 0$, where (x_0, p_{x0}) is a point on the phase planes of the corresponding 2D potentials. This point lies inside the limiting curve, which is the curve containing all the invariant curves of the 2D system. The equation of the limiting curve is

$$\frac{1}{2}p_x^2 + V_{\rm t}(x) = E_2\,, \tag{15}$$

where E_2 is $E_{2\rm tg}$ or $E_{2\rm tl}$. Using this method, we have computed a large number of 3D orbits - about 1000 - with the same initial conditions in both 3D potentials $V_{\rm tg}$ and $V_{\rm tl}$. In particular, as we have in both cases regular regions and only one unified chaotic sea in each $x - p_x$ phase plane, we calculate the maximum value of the LCE by choosing 500 orbits with different and random initial conditions (x_0, p_{x0}, z_0) in the regular regions and 500 orbits with different and random initial conditions (x_0, p_{x0}, z_0) in the chaotic sea in each case. Our numerical calculations indicate that the majority of orbits - about 94.6% - displayed almost the same characteristics, which are the shape of the orbit, the maximum LCE, the $S(w)$ spectrum and the $P(f)$ indicator, while only 5.4% of orbits were different.

Therefore, from the investigation of the 3D potentials, we have arrived at the following conclusions. The mass densities near the center of the elliptical galaxy produced by the potentials are nearly the same. Furthermore, orbits with the same initial conditions in both potentials are very similar and show similar patterns of the maximum LCE, the $S(w)$ spectrum and the $P(f)$ indicator.

Moreover, the percentage of chaotic orbits in both 3D potentials seems to be almost the same. Thus, we conclude that, generally speaking, the properties of motion in both 3D potentials are almost the same.

4 DISCUSSION AND CONCLUSIONS

In this paper we have studied the properties of motion near the center of a triaxial elliptical galaxy described by two different potentials $V_{\rm tg} = V_{\rm g} + V_{\rm n}$ or $V_{\rm tl} = V_{\rm l} + V_{\rm n}$. In fact, $V_{\rm l}$ is an expansion of the potential $V_{\rm g}$ in a Taylor series near the center, up to the terms of fourth degree in the variables, while the potential $V_{\rm n}$ was added for two basic reasons. The first reason is that there is observational evidence that black holes or dense massive nuclei lie in the centers of some elliptical galaxies. The second reason is that with the additional term $V_{\rm n}$, potentials $V_{\rm tg}$ and $V_{\rm tl}$ produce interesting orbital characteristics, such as several families of periodic orbits together with large chaotic regions. In this work we do not have as an objective to provide anything new regarding the properties of motion of these dynamical systems. On the contrary, we use well known potentials and try to compare them by using different kinds of indicators. Our purpose is to show how we can correctly expand a logarithmic potential in a Taylor series to produce a harmonic oscillator. The main result from our research is that despite the fact that the potentials are different, they display almost identical properties of motion. The results obtained using different dynamical indicators are very similar. This means that the Taylor expansion is valid and the harmonic oscillator potential can satisfactorily describe the local motion in the central parts of an elliptical galaxy. On this basis, we provide relations regarding the involved parameters, so that the parameters of the system do not have arbitrary values but rather values which are related to the global logarithmic potential and they have physical meaning.

First we studied the 2D system. The phase planes which were constructed for the two above different potentials were found to be nearly identical. In the next step we studied the properties of orbits with the same initial conditions in both potentials using the maximum LCE, the $S(c)$ spectrum and the $P(f)$ indicator. In all cases the results were very similar. Then we started the study of the 3D system by comparing the mass density in the two potentials $V_{\rm tg}$ and $V_{\rm tl}$. The results have shown very small differences in the mass densities. As in the 2D system we also investigated the properties of orbits in both 3D potentials using the maximum LCE, the $S(w)$ spectrum and the $P(f)$ indicator. The results were once more very similar. Furthermore, our numerical calculations suggest that the percentage of chaotic orbits is about the same in both the above potentials.

Also note that, strictly speaking, potential (1) is a global galactic potential, which describes a triaxial galaxy as a whole, while potential (2) is a local potential, which describes the galaxy only in its central parts. In other words, the description is satisfactory only if relation (4) is valid. Since the two potentials are similar, the orbital behavior of the orbits should be almost identical, while the minor observed differences are caused by the higher order terms of the Taylor expansion. It would be of particular interest to inspect and locate the range of the parameters for which the orbital behavior in both dynamical systems remains the same. Numerical experiments indicate that the results are sensitive to the parameters of the dynamical systems. In particular, we conclude that the properties of motion (2D or 3D) in both potentials $V_{\rm tg}$ and $V_{\rm tl}$ are almost the same only when $1.1 \leq a \leq 1.9, 0.1 \leq b \leq 1.8, 1.8 \leq c_{\rm b} \leq 3.2, 5 \leq M_{\rm n} \leq 25$ and $0.10 \leq c_{\rm n} \leq 0.25$. Numerical calculations not given here show that the properties of motion near the center of potentials (1) and (3) are almost the same. The only difference is that in this case (when the spherical nucleus in not present) we only observe regular motion, while the chaotic orbits if any are negligible. With the additional term $V_{\rm n}$, the two potentials display regular and chaotic motion as well and the properties of motion are again very similar.

Here we must remind the reader that he or she can find the definitions and also some useful theoretical explanations about the $S(c)$ and $S(w)$ dynamical spectrums in Caranicolas & Papadopoulos (2007), in Caranicolas & Zotos (2010) and also in Zotos (2011a). The definition and additional in-

formation regarding the $P(f)$ indicator are given in Karanis & Vozikis (2008). The main drawback of all these methods is that they can only provide qualitative results regarding the regular or chaotic nature of an orbit. Therefore, we must check the shape of the indicator by eye each time in order to characterize an orbit. Nevertheless, these dynamical indicators are very useful as they can provide fast and reliable results. In order to check their validity and reliability in each case (2D and 3D systems), we have compared these qualitative results with a highly accurate and quantitative method, such as the Lyapunov Characteristic Exponent. Our comparison proves that although the outcomes of these spectral methods are qualitative they are also very reliable.

Acknowledgements Stimulating discussions with Professor N. D. Caranicolas during this research are gratefully acknowledged. I would also like thank the anonymous referee for the careful reading of the manuscript and his useful suggestions and comments, which allowed us to improve the quality of the present paper.

References

Alam, S. M. K., & Ryden, B. S. 2002, ApJ, 570, 610
Bak, J., & Statler, T. S. 2000, AJ, 120, 110
Benacchio, L., & Galletta, G. 1980, MNRAS, 193, 885
Benettin, G., Galgani, L., & Strelcyn, J.-M. 1976, Phys. Rev. A, 14, 2338
Bertola, F., & Capaccioli, M. 1975, ApJ, 200, 439
Binney, J., & Tremaine, S. 2008, Galactic Dynamics, Princeton Series in Astrophysics (2nd edition)
Binggeli, B. 1980, A&A, 82, 289
Caranicolas, N. D., & Papadopoulos, N. J. 2007, Astronomische Nachrichten, 328, 556
Caranicolas, N. D., & Zotos, E. E. 2010, New Astron., 15, 427
Contopoulos, G., Grousousakou, E., & Voglis, N. 1995, A&A, 304, 374
Contopoulos, G., Voglis, N., Efthymiopoulos, C., et al. 1997, Celestial Mechanics and Dynamical Astronomy, 67, 293
Davies, R. L., Kuntschner, H., Emsellem, E., et al. 2001, ApJ, 548, L33
Froeschle, C. 1984, Celestial Mechanics, 34, 95
Froeschle, C., Froeschle, C., & Lohinger, E. 1993, Celestial Mechanics and Dynamical Astronomy, 56, 307
Hasan, H., & Norman, C. 1990, ApJ, 361, 69
Hasan, H., Pfenniger, D., & Norman, C. 1993, ApJ, 409, 91
Henon, M., & Heiles, C. 1964, AJ, 69, 73
Illingworth, G. 1977, ApJ, 218, L43
Karanis, G. I., & Vozikis, C. L. 2008, Astronomische Nachrichten, 329, 403
Laskar, J. 1993, Physica D Nonlinear Phenomena, 67, 257
Laskar, J., Froeschlé, C., & Celletti, A. 1992, Physica D Nonlinear Phenomena, 56, 253
Lichtenberg, A. J., & Lieberman, M. A. 1992, Regular and Stochastic Motion (2nd edition, Springer)
Rest, A., van den Bosch, F. C., Jaffe, W., et al. 2001, AJ, 121, 2431
Ryden, B. S. 1996, ApJ, 461, 146
Sandage, A., Freeman, K. C., & Stokes, N. R. 1970, ApJ, 160, 831
Statler, T. S., Emsellem, E., Peletier, R. F., & Bacon, R. 2004, MNRAS, 353, 1
Vincent, R. A., & Ryden, B. S. 2005, ApJ, 623, 137
Voglis, N., & Contopoulos, G. J. 1994, Journal of Physics A Mathematical General, 27, 4899
Zotos, E. E. 2011a, Baltic Astronomy, 20, 77
Zotos, E. E. 2011b, Baltic Astronomy, 20, 339